HHS Public Access

Author manuscript

Nat Commun. Author manuscript; available in PMC 2013 October 16.

Published in final edited form as:

Nat Commun. 2013 ; 4: 1725. doi:10.1038/ncomms2726.

An engineered dimeric protein pore that spans adjacent lipid bilayers

Shiksha Mantri[1], **K. Tanuj Sapra**[1], **Stephen Cheley**[1,2], **Thomas H. Sharp**[3], and **Hagan Bayley**[1,*]

[1]Department of Chemistry, University of Oxford, Oxford OX1 3TA, UK

[3]Department of Physics, University of Oxford, Oxford OX1 3PU, UK

Abstract

The bottom-up construction of artificial tissues is an underexplored area of synthetic biology. An important challenge is communication between constituent compartments of the engineered tissue and between the engineered tissue and additional compartments, including extracellular fluids, further engineered tissue and living cells. Here we present a dimeric transmembrane pore that can span two adjacent lipid bilayers and thereby allow aqueous compartments to communicate. Two heptameric staphylococcal α-hemolysin (αHL) pores were covalently linked in an aligned cap-to-cap orientation. The structure of the dimer, $(\alpha 7)_2$, was confirmed by biochemical analysis, transmission electron microscopy (TEM) and single-channel electrical recording. We show that one of two β barrels of $(\alpha 7)_2$ can insert into the lipid bilayer of a small unilamellar vesicle, while the other spans a planar lipid bilayer. $(\alpha 7)_2$ pores spanning two bilayers were also observed by TEM.

A major challenge in synthetic biology is the construction of tissue-like materials. Lipid vesicles have been used as minimal cells (or protocells)[1–4], but far less work has been done on minimal tissues, i.e. assemblies of small aqueous compartments with tissue-like properties[5]. We have suggested that aqueous droplets connected through droplet interface bilayers[6] might be used to build functional compartmented assemblies, and significant progress has been made in this area[7–9].

An important functional criterion of a minimal cell or tissue is communication with the external environment. Further, in a minimal tissue, the compartments must be able to communicate with each other. To that end, the staphylococcal α-hemolysin (αHL) pore has been used to mediate the transfer of small molecules across the bilayers of lipid vesicles[10].

*Correspondence and requests for materials should be addressed to H.B. (hagan.bayley@chem.ox.ac.uk).

[2]Present address: Alberta Diabetes Institute, Department of Pharmacology, University of Alberta, Edmonton, T6G 2E1, Canada

Author contributions

H.B., S.M. and K.T.S. conceived the ideas. S.M. designed and performed the experiments, analysed the data, and developed the electrical model. K.T.S. helped in the experimental design and data analysis. S.C. helped in the biochemical characterization experiments. T.H.S. performed the TEM experiments and image analysis. S.M., K.T.S and H.B. wrote the manuscript.

Competing Financial Interests

None declared.

The αHL pore can also allow compartments in droplet networks to communicate chemically and electrically with each other and the entire assembly to communicate with the external environment[8].

These examples require individual bilayers to be spanned by protein pores, but it would also be advantageous to be able to connect vesicles or compartmented networks of vesicles through their encapsulating bilayers. Previously described methods such as the drawing of membranous nanotubes to connect vesicles require external micromanipulation techniques[11]. In favourable circumstances, a simpler and self-assembling alternative would be to use a protein that spans two bilayers (Fig. 1a,b), the issue addressed in the present work. Double bilayers are a recurrent feature in nature, and occur in organelles such as mitochondria, chloroplasts and other plastids, autophagosomes and cell nuclei. Both small and large molecules are ferried across the double membranes of organelles by using transiently interacting proteins spanning each of the bilayers, e.g. the TIM/TOM complex of mitochondria[12], or through permanently associated protein complexes spanning the two bilayers, e.g. the nuclear pore complex[13]. A notable example of a protein that spans two bilayers is the gap junction, where the interdigitating extracellular loops of hemi-channels or connexons in individual bilayers are connected by a network of hydrogen bonds and salt bridges to form full channels[14–16].

Inspired by the structure of gap junctions, we have engineered a dimeric αHL pore, $(\alpha 7)_2$, in which two αHL heptamers (α7) are covalently linked by disulfide bonds. $(\alpha 7)_2$ formed spontaneously during the purification of an αHL cysteine mutant that had been designed to allow cap-to-cap coupling. The two β barrels of the construct are able to insert simultaneously into two different bilayers and hence form a conduit between two aqueous compartments (Fig. 1b). Disulfide-bonded tubules have previously been obtained from the hexameric ring of Pseudomonas aeruginosa Hcp1[17] and from the undecameric ring of Bacillus stereothermophilus TRAP[18], but neither of these structures interact with lipid bilayers.

Results

Design of the $(\alpha 7)_2$ pore

Our inspiration for $(\alpha 7)_2$ was the hexameric connexon protein, which forms gap junctions between two adjacent biological cells[14–16]. The flat cap of the heptameric αHL pore (α7)[19] offered the possibility of connecting two α7 units cap-to-cap, to yield a dimer with the bilayer-spanning β barrels pointing away from each other (Fig. 1b). To covalently link the two α7 units, a surface-exposed cap residue, Lys-237, was mutated to cysteine (Fig. 1c,d). The K237C mutation has been studied previously and has no effect on the hemolytic activity of monomeric αHL towards rabbit erythrocytes, which requires heptamer formation, even when the cysteine is modified with a bulky chemical group[20] (Supplementary Fig. S1a). The unitary conductance of the heptameric (α7) K237C pore in planar lipid bilayers was 857±6pS (mean±s.e.m; n=169, N=9, where n is number of individual events in N independent experiments) in 1M KCl, 25mM Tris.HCl, 50μM EDTA, pH8.0, which is similar to the value for wild-type (WT) α7[21].

Molecular dynamics (MD) simulations of $(\alpha 7)_2$

The structural viability of a cap-to-cap $(\alpha 7)_2$ dimer of the K237C mutant was evaluated by MD simulations. Two α7 units were docked cap-to-cap in PyMOL, and disulfides were formed between cysteine thiol pairs in GROMACS[22]. $(\alpha 7)_2$ was solvated in a buffer containing 500mM NaCl, and a 1ns all-atom MD simulation was performed. In the energy minimized structure of $(\alpha 7)_2$, the seven disulfides did not provoke steric clashes between the other interface residues (Supplementary Fig. S2a). Energy analysis revealed favorable overall electrostatic interactions and Lennard-Jones potential energy between the α7 caps (Supplementary Fig. S2b).

$(\alpha 7)_2$ forms spontaneously during K237C purification

A D8H6 peptide tag was placed at the C terminus of the αHL K237C monomer (α1; M_{app} 33,200) to aid purification by immobilized metal affinity chromatography (Ni-NTA agarose). After separation of K237C/D8H6 from the *E. coli* cell lysate, a mixture of α1, monomer dimer $(\alpha 1)_2$, α7 and a species of M_{app}≈190,000 was obtained. We anticipated that the latter was $(\alpha 7)_2$. The D8H6 tag on the C terminus of αHL promotes premature oligomerization of WT α1 into α7 (Stephen Cheley, unpublished results). Therefore, we believe that α1 spontaneously oligomerizes to α7, which subsequently forms $(\alpha 7)_2$ during purification.α7 is known to be stable in the sample buffer used for SDS-PAGE[23]. The spontaneously oligomerized K237C α7 carried seven D8H6 tags, and hence considerably more negative charge compared with WT α7. The reduced hydrodynamic radius of the folded α7 structure in SDS and the additional negative charges per heptamer caused α7 to migrate quickly during SDS-PAGE[24] with M_{app}≈120,000, rather than M_{app}≈230,000 based on its molecular mass. The dimer, $(\alpha 7)_2$, too would be expected to migrate more quickly than anticipated based on its mass, and therefore we attributed the M_{app}≈190,000 band, lying above the α7 band, to $(\alpha 7)_2$.

Structural characterization of $(\alpha 7)_2$

To confirm that the M_{app}≈190,000 species in SDS-polyacrylamide gels (Fig. 2a) was $(\alpha 7)_2$, formed of α7 units linked through disulfide bonds, we extracted the band from a gelin 10mM Tris.HCl, 1mM EDTA, pH8.0, and treated the protein with 3M βME for 15min at 25°C, which yielded α7 only (*lane 4*, Fig. 2b). Upon heating the M_{app}≈190,000 species at 95°C for 10min in the absence of a reducing agent, it dissociated into two species, which were identified as α1 and $(\alpha 1)_2$ (*lane 3*, Fig. 2b). The relative intensities of the α1 and $(\alpha 1)_2$ bands were 18 and 17 absorbance units, respectively. Therefore, $(\alpha 7)_2$ (M_{app}≈190,000) is composed of α1 and $(\alpha 1)_2$ in a ratio of 2:1 (mol/mol). When $(\alpha 7)_2$ (M_{app}≈190,000) was treated with 3M βME for 15min at 25°C, followed by heating in 3M βME at 95°C for 10min, only α1 was formed (*lane 5*, Fig. 2b,c, Supplementary Fig. S1b). These experiments showed that the cysteines introduced into the cap domain had been oxidized to form disulfide bonds and thereby convert α7 to $(\alpha 7)_2$.

$(\alpha 7)_2$ might be formed from structures other than a precisely aligned cap-to-cap structure (Fig. 1b), because of the different possible cross-linking patterns between the α7 units (Supplementary Fig. S3, Supplementary note 1). However, when theα7 units are linked at three or more positions, i.e. by three or more disulfide bonds, only the aligned structure of

$(\alpha7)_2$ is possible (Supplementary Fig. S3e). From the ratio of the band intensities of α1 and $(\alpha1)_2$ in heat dissociated $(\alpha7)_2$ (Fig. 2b), we deduced that on average ~3.3 out of the 7 cysteines in each α7 unit were oxidized to form disulfide linkages, and hence the majority of the $(\alpha7)_2$ were aligned along a central axis (Fig. 1b).

The cap-to-cap structure of $(\alpha7)_2$ was further investigated by examination of $(\alpha7)_2$ and α7 by TEM. α7 was observed only as ring-shaped particles of diameter 8.1±0.1nm (mean ±s.e.m.; *n*=52) (data not shown), in accord with previous reports[19,25,26]. In contrast, both side views and rings were observed in the case of $(\alpha7)_2$ in a roughly 2:1 ratio (*n*=399, *N*=4) (Fig. 2d,e). The $(\alpha7)_2$ rings looked similar to those of α7 with an average diameter 7.8±0.1nm (mean±s.e.m.; *n*=131) (Fig. 2g, Supplementary Fig. S4). Offset $(\alpha7)_2$ structures (Supplementary Fig. S3a–d) could not be discerned amongst the aligned cap-to-cap structures in the images of the rings (Fig. 1b, Supplementary Fig. S3e). The side views of $(\alpha7)_2$ revealed elongated particles with an average length of 19.6±0.2nm (mean±s.e.m.; *n*=268) and average width of 8.4±0.1nm (mean±s.e.m.; *n*=96) (Fig. 2d,f), in agreement with the predicted dimensions of a cap-to-cap dimer (Fig. 1b).

$(\alpha7)_2$ is a correctly folded structure

Proteinase K cleaves at the glycine-rich central domain and near the N terminus of α1[27], regions inaccessible in the α7 structure[28]. α7 extracted from an SDS gel was treated with proteinase K (0.5mg mL^{-1}) and subsequently heated at 95°C for 10min, yielding untruncated α1, confirming the previous findings (*lanes 5, 6*, Supplementary Fig. S5). $(\alpha7)_2$ treated in the same way, yielded intact α1 and $(\alpha1)_2$, and was reduced to intact α7 upon treatment with 3M βME for 15min at 25°C (*lanes 1–4*, Supplementary Fig. S5). Therefore $(\alpha7)_2$, like α7 has a compact folded structure.

Conductance of $(\alpha7)_2$ suggests it is a longer pore than α7

TEM showed that $(\alpha7)_2$ inserted into the bilayers of POPC liposomes when mixed in a lipid to protein ratio of 100:1 (w/w) (Fig. 3a). The average length of $(\alpha7)_2$ molecules protruding out of single liposomes was 17.0±0.4nm (mean±s.e.m.; *n*=131), close to the value of 15nm expected from the molecular model (Fig. 1b). As evidenced by electrical recordings, $(\alpha7)_2$ readily inserted into planar lipid bilayers (Fig. 3b,c). We surmise that one of the α7 β barrels (which we call the *trans*-α7 half of the structure) penetrates the bilayer, while the other α7 unit (*cis*-α7) is surrounded by buffer and perhaps stabilized by residual traces of SDS (Fig. 3b). Histograms of the unitary pore currents (I_o)of $(\alpha7)_2$ at each of three potentials, +50mV, +100mV and +160mV, showed at least two populations (red and green, Fig. 3c,d; Supplementary Fig. S6) suggesting the existence of more than one $(\alpha7)_2$ structure. A double Gaussian function was used to fit the I_o histogram of $(\alpha7)_2$. At +50mV, 75% of the $(\alpha7)_2$ pores had a mean I_o of 27±4pA(mean±standard deviation(stdev); *n*=284, *N*=18; 1M KCl, 25mM Tris.HCl, 50μM EDTA, pH8.0) (Fig. 3d, red peak), which is ~64% of the I_o value of α7 of 42±4pA(mean±stdev; *n*=169, *N*=9). The mean I_o of the remaining 25% of the $(\alpha7)_2$ pores was 42±4pA, (mean±stdev; *n*=93, *N*=18) (Fig. 3d, green peak), which corresponds to the value for α7. Therefore, the α7 units in the latter $(\alpha7)_2$ structures may be offset (Supplementary Fig. S3a-c, Supplementary note 1). The lower conductance of 75% of the $(\alpha7)_2$ pores (±4%: ±95% confidence interval, see Supplementary methods, Fig. 3d, red

peak) is consistent with a pore that is longer than α7 (Supplementary Fig. S3d,e) and most likely reflects a precisely aligned cap-to-cap orientation.As the probability of insertion of the aligned and misaligned $(\alpha7)_2$ structures (Supplementary Fig. S3) into the planar lipid bilayer must be similar based on their similar structures, the conductance distribution implies that the major species present is the aligned $(\alpha7)_2$ structure.

The I–V characteristics of the $(\alpha7)_2$ and α7 pores differed (Fig. 3e). The rectification ratios diverged most strikingly at positive potentials. For example, (I_{+100} /I_{-100}) was 1.29±0.02 (mean±s.e.m.; *N*=5) for α7 and 1.05±0.05 (mean±s.e.m.; *N*=8) for $(\alpha7)_2$. Indeed, the I–V characteristics for $(\alpha7)_2$ were roughly ohmic from negative to positive applied potentials, which is consistent with a symmetrical pore structure (Fig. 3e).

Cyclodextrin binding to $(\alpha7)_2$ confirms presence of two β barrels

The functional and hence the structural characteristics of $(\alpha7)_2$ were further investigated by determining the binding kinetics of the α7 pore adapter, γ cyclodextrin (γCD)[29]. Large cyclodextrins such as γCD become lodged near residue N139 in the α7 β barrel for hundreds of milliseconds, which can be detected electrically as characteristic current blockades[30]. As reported previously, γCD bound to α7 from the *trans* side of the bilayer only and produced a blockade of 66±1% of I_o (percent block±s.e.m.; *n*=17,354, *N*=6) at +50mV (Fig. 4a–d). Under the same conditions, γCD blocked $(\alpha7)_2$ from both the *trans* and the *cis* sides of the bilayer (Fig. 4e–h). Blocking from the *trans* side was observed with 100% success (*n*=33, *N*=15, where *n* is number of pores in *N* experiments), and from the *cis* side in 50 out of 56 pores examined (89±8%; percentage of pores blocked±95% confidence interval; *n*=56, *N*=19) (Fig. 4e–h). Hence, $(\alpha7)_2$ contains two γCD binding sites, one facing each side of the bilayer, which is consistent with the presence of two symmetrically placed β barrels.

γCD, when added to the *cis* side of a bilayer containing $(\alpha7)_2$ (*cis* γCD binding), produced a smaller block of I_o than *trans* γCD binding (Table 1). For example, at +50mV, *cis* γCD gave a 15±1% blockade of I_o (percentage block±s.e.m., *n*=22,344, *N*=12; where *n* is the total number of events in *N* experiments) as compared to 55±2% (*n*=11,068, *N*=7) for *trans* γCD binding. The association rate constants (k_{on}) were similar for *cis* and *trans* γCD binding (Table 1). However, the dissociation rate constants (k_{off}) for *cis* γCD were approximately twice the values determined for *trans* γCD binding (Table 1). The physical origins of a smaller block of I_o and the slightly weaker *cis* γCD binding compared to *trans* γCD binding with $(\alpha7)_2$ might be attributed respectively to a leak in the structure (Supplementary Fig. S3e, Supplementary note 1) and a less compact structure of the *cis*-α7 β barrel in $(\alpha7)_2$ owing to the absence of a lipid bilayer.

When γCD was added to both the *cis* and the *trans* sides of the bilayer, events were observed that could be attributed to binding to either the *cis* α7 unit or the *trans* α7 unit, or to both sites at the same time, e.g. at +50mV, simultaneous block, 61±1%; *cis* block 15±2%; *trans* block, 57±1%, (percentage block of I_o±s.e.m.; *n*=1121, 4183, 3737 respectively, *N*=6). The simultaneous block was preceded by and followed by either a *cis* or a *trans* block (Fig. 4i,j).

Phosphate binding confirms aligned structure of M113R $(\alpha 7)_2$

We also examined phosphate anion (P_i), a *cis* (cap side) blocker of certain α7 mutants[31]. At +20mV, P_i blocked the α7 pore formed from M113R, when added to the *cis* compartment (Fig. 5a–c). The α7 pore remained open when P_i was added to the *trans* compartment (data not shown). We hypothesized that a precise cap-to-cap $(\alpha 7)_2$, made from the barrel mutant M113R/K237C/D8H6 (MR), would not show P_i blockades as there would be no available entrance for P_i ions (Fig. 5d,e). 48 of 65 MR $(\alpha 7)_2$ pores, i.e. 74±11% (percentage of pores examined±95% confidence interval), were not blocked by P_i added from the *cis* side. The population (74%) of $(\alpha 7)_2$ structures obtained from MR with aligned caps, as deduced from P_i blocking experiments, corresponded well with the value of 75±4% determined by conductance measurements on K237C pores (n=377, N=18) (Fig. 3d). These results in conjunction with the γCD binding and TEM experiments suggest that a majority of $(\alpha 7)_2$ pores have an aligned cap-to-cap structure.

Of the 65 MR $(\alpha 7)_2$ pores examined, 17 were blocked by P_i in a similar manner to MR α7 (Supplementary Fig. S7). 12 of these 17 MR $(\alpha 7)_2$ pores, i.e. 71±22% (percentage of pores examined±95% confidence interval) had unitary conductance values similar to MR α7. These pores may have had *cis*-α7 units that were misaligned or misfolded in such a way that P_i ions could enter into the *trans*-α7 unit from the *cis* compartment. Indeed, when we examined MR $(\alpha 7)_2$ samples that had been freeze-thawed three times, we found that the mean I_o was increased by 2pA and that P_i blocking occurred with 14 out of 25 pores (Supplementary Fig. S8, Supplementary note 2).

$(\alpha 7)_2$ inserts into two lipidbilayers simultaneously

The insertion of $(\alpha 7)_2$ into bilayers was examined by TEM. $(\alpha 7)_2$ was mixed with unilamellar egg-PC liposomes or 10 mol% POPG:POPC liposomes in a lipid-to-protein ratio of 100:1 and 20:1(w/w),respectively. To prevent aggregation of liposomes, POPG was added to POPC to make liposomes with a net negative charge. The insertion of one end of $(\alpha 7)_2$ into individual liposomes (Fig. 3a) and the simultaneous insertion of both ends into each of two liposomes were observed (Fig. 6a,b). The average length of $(\alpha 7)_2$ structures spanning two liposomes was 12.3±0.7nm (mean±s.e.m.; n=15), close to the value of 10nm expected from the molecular model (Fig. 1b).

To investigate simultaneous insertion into two bilayers by electrical recording, we determined whether the exposed *cis* β barrel of $(\alpha 7)_2$ in a planar lipid bilayer could insert into a liposome. First, we found that pre-incubation with unilamellar liposomes (25mg mL^{-1} DPhPC, 1M KCl, 25mM Tris.HCl, 50μM EDTA, pH8.0; filter cut-off, 100nm diameter) decreased the rate of insertion of $(\alpha 7)_2$ (50μg mL^{-1}) into planar lipid bilayers by >100 fold, presumably because both β barrels of $(\alpha 7)_2$ had inserted irreversibly into the liposomes. Next, with $(\alpha 7)_2$ already inserted into a planar lipid bilayer, liposomes were added to the *cis* compartment and a permanent current blockade of 23±1% (percentage of I_o±s.e.m.; N=12) was observed at +50mV in 12 out of 14 experiments (Fig. 6c,d). After liposome block, $(\alpha 7)_2$ had a lower unitary conductance over a wide range of applied potentials: −200 to +200mV (Supplementary Fig. S9a), while its rectification properties were little changed (Supplementary Fig. S9b). For example, at 100mV, the rectification ratio (I_{+100} /I_{-100}) of an

$(\alpha7)_2$ pore inserted into a liposome was 0.96±0.03 (mean±s.e.m., *N*=3), as compared to 1.05±0.05 (mean±s.e.m., *N*=8) for $(\alpha7)_2$ in the absence of liposomes. The residual current might be explained by one of two scenarios: either by assuming that the attached liposome is porous because it is penetrated by additional $(\alpha7)_2$ pores or by a leak current within the $(\alpha7)_2$ pore in the planar bilayer (Supplementary Fig. S10). However, the number of $(\alpha7)_2$ protein molecules present was much smaller than the number of liposomes in the *cis* compartment, which points against the first possibility. Further, the consistent magnitude of current blockades caused by liposome insertion favors the second scenario (Supplementary note 3).

Cis γCD blockades cease after liposome insertion

To confirm that the observed blockade of $(\alpha7)_2$ arose because of *cis*-α7 barrel insertion into a liposome, γCD was added to the *cis* compartment before and after $(\alpha7)_2$ liposome insertion. When γCD was added after insertion of $(\alpha7)_2$ into a liposome, γCD binding events were not observed (*N*=6), confirming that the *cis*-α7 barrel entrance was inaccessible (Fig. 6e). If γCD was already present in the *cis* compartment before the addition of liposomes, the blocking events ceased upon insertion of the *cis*-α7 unit into a liposome (*N*=4, Fig. 6f). By contrast, if γCD was present on the *trans* side before the addition of liposomes, γCD blockades continued even after the insertion of the *cis*-α7 unit into a liposome (Fig. 6g,h). However, the magnitude of current blockades arising from *trans* γCD binding changed from 60±1% (mean±s.e.m.) before insertion to 56±1% after insertion (*n*=4144, *N*=5) (Supplementary note 3). Therefore, the *cis*-α7 unit could insert into a liposome, which then occluded the barrel entrance, but produced no effect on the binding properties of the *trans*-α7 unit, which spanned the planar lipid bilayer.

Electrical model of $(\alpha7)_2$ explains its observed properties

To explain the electrical properties of $(\alpha7)_2$ and the current blockades observed with γCD and liposomes, an electrical model of the pore was constructed (Supplementary note 3). The model assumes that the *cis*-α7 and *trans*-α7 units are resistors, represented by R_c and R_t, respectively (Supplementary Fig. S11a,b). The values of R_c and R_t were set to experimentally determined values of the unitary resistance of α7 at −50mV and +50mV, respectively. The value for R_c was taken at −50mV, because the orientation of the *cis*-α7 unit is the opposite of that of *trans*-α7, and the opposite of that in our usual sign convention. In any event, both values are 1.2GΩ, because rectification of α7 is weak at low potentials (Fig. 3e). Therefore, the resistance of $(\alpha7)_2$ should be 2.4GΩ. However, the experimentally determined resistance of the cap-to-cap $(\alpha7)_2$ pores (R_d) was 1.8GΩ, which implies that a leak in the structure of $(\alpha7)_2$ contributes to the measured conduction through the $(\alpha7)_2$ pore. The leak could be due to a flow of ions in between the *cis*-α7 and *trans*-α7 units or through aqueous channels within the α1 subunits (Supplementary Fig. S3e). To account for the leak current, an additional resistor (R_L) was placed in parallel to R_c. By using the experimentally determined values ofR_d=1.8GΩ, R_c=1.2GΩ and R_t=1.2GΩ, R_L was calculated to be 1.2GΩ at +50mV.

Current blockades by γCD can be explained with the same electrical model by including an additional resistance R_{CD}. A switch is included to contend with transient binding, i.e. the

pore with γCD bound has the switch open, while the unoccupied pore has the switch closed (Supplementary Fig. S11c–f). The overall resistances of the model circuits were calculated (Supplementary note 3). At +50mV, the blockades in I_o due to *cis* and *trans* γCD binding are 14% and 56%, respectively (Supplementary Fig. S11d,e; Supplementary Table S1), which match the experimental values of 15±1% and 55±2% (Table 1). Similarly, the calculated current blockade for simultaneous binding of γCD to both the *cis* and *trans* sites is 59% (Supplementary Fig. S11f), which is similar to the experimental value of 61±1% at +50mV. The value of the current block expected upon liposome insertion at +50mV is computed to be 25% (Supplementary Fig. S12a), which agrees well with the experimental liposome blockade of 23±1%. The *trans* γCD blockade when the *cis* α7unit was inserted into a liposome is 49% (Supplementary Fig. S12b) according to the model, which is reasonably close to the experimental value of 56±1%. Theoretical values of R_L and *cis* and *trans* γCD blocking were calculated by using equations (S3)–(S9) (Supplementary note 3) at +100mV and −50mV. The predicted values (Supplementary Table S1) correlated well with the experimentally observed values (Table 1). These correlations imply that the calculated value of R_L is correct at all the potentials examined. Comparing the values of R_L and R_c, we infer that the leak amounts to 50%, and 60%, of the total current going into the *trans*-α7 unit at +50mV and −50mV, and at +100mV, respectively.

Discussion

We have used protein engineering to build a dimeric pore $(\alpha7)_2$ that, like eukaryotic gap junctions, can span two lipid bilayers to form a conductive pathway. The structure of $(\alpha7)_2$ was characterized by biochemical assays, TEM and single channel electrical recordings. The majority of the $(\alpha7)_2$ comprise two α7 heptamers linked cap-to-cap in a fully aligned fashion through cysteine residues at position 237 (Fig. 1b–d). We confirmed the double β barrel structure of $(\alpha7)_2$ by investigating the interactions of γCD, which bound to the two β barrels of $(\alpha7)_2$ independently. Single channel electrical measurements showed that the β barrels of a $(\alpha7)_2$ pore could span simultaneously a planar lipid bilayer and the bilayer of a small unilamellar lipid vesicle. The bridging of two lipid vesicles by $(\alpha7)_2$ was also observed by electron microscopy.

This paper describes the best attempt so far at the rational design and characterization of a pore that is able to connect adjacent two lipid bilayers. Despite the leak at the cap interface, we believe that the $(\alpha7)_2$ pore is useful in its present form, e.g. for electrical communication across minimal tissues. Further, because the defect has been fully characterized, it should be possible to remedy it in future work. For example, additional disulfide bonds and electrostatic interactions might pull the heptamers closer together, or a covalently attached polymer skirt at the cap interface might reduce ion flow.

Extensive studies have shown that the heptameric αHL pore can be engineered to produce a versatile assortment of functionalized pores, with altered properties including size selection, rectification, triggered activity, reversible gating and blocker binding[7,29,31–33]. If such properties were introduced into $(\alpha7)_2$, the dimeric pore might be used in a variety of contexts. For example, minimal cells endowed with a light-activated $(\alpha7)_2$ might be used to inject doses of therapeutic or cytotoxic agents directly into living cells[34,35].

Minimal cells connected through $(\alpha7)_2$ might be used to form minimal tissues, i.e. collections of communicating compartments (Fig. 1a, upper panel). A different form of minimal tissue formed of networks of aqueous droplets connected by single lipid bilayers has been under development in our laboratory[6–9]. Recently, it has been demonstrated that these networks can be encapsulated in small oil drops so that they are separated from the external environment through single bilayers[8]. These encapsulated droplet networks might be connected to each other through bridges such as $(\alpha7)_2$ to form extended tissue-like droplet networks (Fig. 1a, lower panel). As in the case of gap junctions[36], thousands of $(\alpha7)_2$ pores might be required to transfer substantial amounts of small molecules across the protocells in minimal tissues.

Because the αHL pore is capable of spanning the plasma membranes of mammalian cells[34], it also follows that $(\alpha7)_2$ might be used to integrate minimal tissues with living cells and tissues by permitting chemical and electrical communication between them, and thereby open up further frontiers in tissue engineering (Fig. 1a, lower panel).

Methods

Computational modelling of $(\alpha7)_2$

Two α7 subunits with the K237C mutation were docked in a cap-to-cap orientation in PyMOL (Schrodinger) such that the cysteines of each α7 aligned with the other. The topology file was generated using GROMACS version 4.0 (www.gromacs.org), and edited to introduce position restraints on the cysteine thiol atoms. The distance between sulfur atoms the aligned cysteines was fixed at 0.2nm, which is the S-S bond length. An all-atom MD simulation was performed on the docked structure for 1ns in 500mM NaCl buffer using the OPLS-AA/L all-atom force field. The integration time step was 2 fs with an all-bonds constraint. The Particle Mesh Ewald (PME) method[37] was used to compute long-range electrostatics interactions and the short-range electrostatic cut-off was kept at 1nm with a Fourier spacing of 0.32. Steric clashes were visualized by using a PyMOL script (show_bumps.py, Thomas Holder) with a van der Waals radius cut-off of 0.3Å.

Expression and purification of $(\alpha7)_2$ and the mutant M113R

The K237C mutation was introduced into an αHL gene with a D8H6 tag at the C terminus, contained within a pT7 vector[38], by mutagenic PCR followed by homologous recombination in XL10-Gold ultracompetent *E. coli* cells (Agilent). The sequences of the primers used in the forward and reverse PCR mutagenesis reactions were 5′-CTATGGATAGATGCGCATCCAAACAACAAACAAATATAG (forward primer) and 5′-CAGAAGTGGTCCTGCAACTTTAT (reverse primer, and 5′-CTATATTTGTTTGTTGTTTGGATGCGCATCTATCCATAG (reverse primer) and 5′-ATAAAGTTGCAGGACCACTTCTG (forward primer), respectively. Rosetta (DE3) pLysS competent cells (Novagen) were used for protein expression. The αHL proteins α1, $(\alpha1)_2$, α7 and $(\alpha7)_2$ were observed in the cell lysate and purified by Ni^{2+}-NTA chromatography. α7 and $(\alpha7)_2$ were further purified by extraction from SDS-polyacrylamide gels (Supplementary Methods).

Proteinase K assay

Proteinase K (50μg mL^{-1}, 500μg mL^{-1} and 5mg mL^{-1}) was added to purified $(\alpha7)_2$ (1:9 v/v) and incubated for 5min at 25°C, when phenylmethylsulfonyl fluoride (PMSF) was added to a final concentration of 2mM to inhibit the protease. The samples were analysed by using 10% w/v bis-tris SDS-polyacrylamide gel electrophoresis (Bio-Rad).

Single-channel electrical recording

All electrical recordings were done by using planar lipid bilayers formed from 2-diphytanoyl phosphatidylcholine (DPhPC, Avanti Polar Lipids) across a 125-μm aperture in a 30 μm-thick Teflon film with 1M KCl, 25mM Tris.HCl, 50μM EDTA, pH8.0 as the electrolyte. The αHL proteins were added to the electrically grounded compartment, termed '*cis*' (Fig. 3b). Ag/AgCl electrodes were used to apply a bias potential, given as $V_{trans} - V_{cis}$. The electrical current was amplified with a patch-clamp amplifier (Axopatch 200B, Axon Instruments), and acquired with a 1 *k*Hz filter at a sampling frequency of 10 *k*Hz. The electrical recordings were post-filtered with low pass 100 Hz Bessel filter. Experiments reported in the paper were performed with proteins aliquots that had not been freeze-thawed more than once. All chemicals were purchased from Sigma, unless specified otherwise.

Phosphate (P_i) binding experiments

0.5M stocks of sodium dihydrogen phosphate (NaH_2PO_4) and disodium hydrogen phosphate (Na_2HPO_4) were mixed to prepare 0.5M sodium phosphate, pH8.0. The 0.5M sodium phosphate stock was added to the *cis* or *trans* sides of the bilayer to give a final concentration of 10mM phosphate. The P_i binding experiments were performed with fresh aliquots of $(\alpha7)_2$ that had been stored at −80°C, and never thawed.

Preparation of liposomes

Lipids (25 mg in each case: 1,2-diphytanoyl phosphatidylcholine (DPhPC), 1-palmitoyl-2-oleoyl-sn-glycero-3-phosphocholine (POPC), 1-palmitoyl-2-oleoyl-sn-glycero-3-phospho-(1′–*rac*-glycerol) (POPG) and L-α-phosphatidylcholine (95%) (egg-PC), Avanti Polar Lipids) were dissolved in chloroform (1mL). The stocks of POPC and POPG were mixed to give a molar ratio of POPC:POPG of 9:1. The lipid solutions were dried under a stream of nitrogen, and kept under high vacuum in a desiccator for 3 to 4h. The dried lipids were suspended in rehydration buffer (1mL of 1M KCl, 25mM Tris.HCl, 50μM EDTA, pH8.0), and extruded through two 0.1 μm polycarbonate membranes to obtain unilamellar liposomes. For electrical recordings, liposomes (50 or 100μL) were added to 1mL recording buffer in the *cis* compartment.

Electron microscopy and image processing

To obtain images of $(\alpha7)_2$ inserted into liposomes, $(\alpha7)_2$ (50μg mL^{-1}) was mixed with egg-PC or 10 mol% POPG:POPC liposomes at lipid to protein ratios of 100:1 or 20:1 (w/w), respectively. After incubation for 15 to 60min, $(\alpha7)_2$ was applied to freshly glow-discharged continuous-carbon grids and left to adsorb for 1min. After blotting, either 2% (w/v) uranyl acetate or NanoVan® (Nanoprobes, Inc., USA) was used as a negative stain and applied to the grid for ~15s. Grids were imaged at either 120kV (NanoVan) or 80kV (uranyl acetate)

with a Tecnai T12 transmission electron microscope fitted with a tungsten filament and a BioTWIN lens. Micrographs were recorded on an Eagle 4k×4k CCD camera with a final pixel size of 1.675Å/pixel at a nominal magnification of ×52k. All image processing was performed using EMAN2[39]. A total of 2,748 particles were selected semi-automatically by using e2boxer and binned by 2. CTF parameters were determined using e2ctf, followed by phase flipping and high-pass filtering. Reference-free class averages were generated assuming no symmetry using e2refine2d.

Supplementary Material

Refer to Web version on PubMed Central for supplementary material.

Acknowledgments

The authors thank L. Höfler and L. Harrington for help with computational modelling and L. Kong for general discussions. S.M. acknowledges the support of a Clarendon scholarship (Oxford University Press). K.T.S. acknowledges support from the European Commission in the form of a Marie Curie Intra-European Fellowship. This work was supported by grants from the National Institute of Health and Oxford Nanopore Technologies.

References

1. Oberholzer T, Wick R, Luisi PL, Biebricher CK. Enzymatic RNA replication in self-reproducing vesicles: an approach to a minimal cell. Biochem Biophys Res Commun. 1995; 207:250–257. [PubMed: 7531971]
2. Szostak JW, Bartel DP, Luisi PL. Synthesizing life. Nature. 2001; 409:387–90. [PubMed: 11201752]
3. Noireaux V, Bar-Ziv R, Godefroy J, Salman H, Libchaber A. Toward an artificial cell based on gene expression in vesicles. Phys Biol. 2005; 2:P1–8. [PubMed: 16224117]
4. Kurihara K, et al. Self-reproduction of supramolecular giant vesicles combined with the amplification of encapsulated DNA. Nat Chem. 2011; 3:775–81. [PubMed: 21941249]
5. Woolfson DN, Bromley EHC. Synthetic biology: a bit of rebranding, or something new and inspiring? The Biochemist. 2011; 33:19–25.
6. Holden MA, Needham D, Bayley H. Functional bionetworks from nanoliter water droplets. J Am Chem Soc. 2007; 129:8650–8655. [PubMed: 17571891]
7. Maglia G, et al. Droplet networks with incorporated protein diodes show collective properties. Nat Nanotechnol. 2009; 4:437–40. [PubMed: 19581896]
8. Villar G, Heron A, Bayley H. Formation of droplet networks that function in aqueous environments. Nat Nanotechnol. 2011; 6:803–808. [PubMed: 22056724]
9. Sapra KT, Bayley H. Lipid-coated hydrogel shapes as components of electrical circuits and mechanical devices. Sci Rep. 2012; 2:848. [PubMed: 23152939]
10. Noireaux V, Libchaber A. A vesicle bioreactor as a step toward an artificial cell assembly. Proc Natl Acad Sci. 2004; 101:17669–74. [PubMed: 15591347]
11. Jesorka A, et al. Generation of phospholipid vesicle-nanotube networks and transport of molecules therein. Nat Protoc. 2011; 6:791–805. [PubMed: 21637199]
12. Schmidt O, Pfanner N, Meisinger C. Mitochondrial protein import: from proteomics to functional mechanisms. Nat Rev Mol Cell Biol. 2010; 11:655–67. [PubMed: 20729931]
13. D'Angelo MA, Hetzer MW. Structure, dynamics and function of nuclear pore complexes. Trends Cell Biol. 2008; 18:456–66. [PubMed: 18786826]
14. Evans WH, Martin PE. Gap junctions: structure and function. Mol Membr Biol. 2002; 19:121–36. [PubMed: 12126230]
15. Maeda S, et al. Structure of the connexin 26 gap junction channel at 3.5 A resolution. Nature. 2009; 458:597–602. [PubMed: 19340074]

16. Nakagawa S, Maeda S, Tsukihara T. Structural and functional studies of gap junction channels. Curr Opin Struct Biol. 2010; 20:423–30. [PubMed: 20542681]
17. Ballister ER, Lai AH, Zuckermann RN, Cheng Y, Mougous JD. In vitro self-assembly of tailorable nanotubes from a simple protein building block. Proc Natl Acad Sci. 2008; 105:3733–8. [PubMed: 18310321]
18. Miranda FF, et al. A self-assembled protein nanotube with high aspect ratio. Small. 2009; 5:2077–84. [PubMed: 19562822]
19. Song L, et al. Structure of staphylococcal alpha-hemolysin, a heptameric transmembrane pore. Science. 1996; 274:1859–1865. [PubMed: 8943190]
20. Walker B, Bayley H. Key residues for membrane binding, oligomerization, and pore-forming activity of staphylococcal a-hemolysin identified by cysteine scanning mutagenesis and targeted chemical modification. J Biol Chem. 1995; 270:23065–71. [PubMed: 7559447]
21. Gu LQ, Cheley S, Bayley H. Prolonged residence time of a noncovalent molecular adapter, beta-cyclodextrin, within the lumen of mutant alpha-hemolysin pores. J Gen Physiol. 2001; 118:481–94. [PubMed: 11696607]
22. Hess B, Kutzner C, van der Spoel D, Lindahl E. GROMACS 4: Algorithms for highly efficient, load-balanced, and scalable molecular simulation. J Chem Theory Comput. 2008; 4:435–447. [PubMed: 26620784]
23. Bhakdi S, Füssle R, Tranum-Jensen J. Staphylococcal alpha-toxin: oligomerization of hydrophilic monomers to form amphiphilic hexamers induced through contact with deoxycholate micelles. Proc Natl Acad Sci. 1981; 78:5475–5479. [PubMed: 6272304]
24. Kleinschmidt JH, Wiener MC, Tamm LK. Outer membrane protein A of E. coli folds into detergent micelles, but not in the presence of monomeric detergent. Protein Sci. 1999; 8:2065–71. [PubMed: 10548052]
25. Füssle R, et al. On the mechanism of membrane damage by Staphylococcus aureus a-toxin. J Cell Biol. 1981; 91:83–94. [PubMed: 6271794]
26. Gouaux JE, et al. Subunit stoichiometry of staphylococcal alpha-hemolysin in crystals and on membranes: a heptameric transmembrane pore. Proc Natl Acad Sci. 1994; 91:12828–31. [PubMed: 7809129]
27. Walker BJ, Krishnasastry M, Zorn L, Bayley H. Assembly of the oligomeric membrane pore formed by staphylococcal alpha-hemolysin examined by truncation mutagenesis. J Biol Chem. 1992; 267:21782–86. [PubMed: 1400487]
28. Cheley S, et al. Spontaneous oligomerization of a staphylococcal alpha-hemolysin conformationally constrained by removal of residues that form the transmembrane beta barrel. Protein Eng. 1997; 10:1433–43. [PubMed: 9543005]
29. Gu LQ, Braha O, Conlan S, Cheley S, Bayley H. Stochastic sensing of organic analytes by a pore-forming protein containing a molecular adapter. Nature. 1999; 398:686–690. [PubMed: 10227291]
30. Gu LQ, Cheley S, Bayley H. Capture of a single molecule in a nanocavity. Science. 2001; 291:636–640. [PubMed: 11158673]
31. Cheley S, Gu LQ, Bayley H. Stochastic sensing of nanomolar inositol 1,4,5-trisphosphate with an engineered pore. Chem Biol. 2002; 9:829–838. [PubMed: 12144927]
32. Bayley H, Cremer PS. Stochastic sensors inspired by biology. Nature. 2001; 413:226–230. [PubMed: 11557992]
33. Astier Y, Bayley H, Howorka S. Protein components for nanodevices. Curr Opin Chem Biol. 2005; 9:576–84. [PubMed: 16257572]
34. Eroglu A, et al. Intracellular trehalose improves the survival of cryopreserved mammalian cells. Nat Biotechnol. 2000; 18:163–167. [PubMed: 10657121]
35. Tran SL, Puhar A, Ngo-Camus M, Ramarao N. Trypan blue dye enters viable cells incubated with the pore-forming toxin HlyII of Bacillus cereus. PLoS One. 2011; 6:e22876. [PubMed: 21909398]
36. Goodenough DA, Paul DL. Gap junctions. Cold Spring Harb Perspect Biol. 2009; 1:a002576. [PubMed: 20066080]
37. Essmann U, et al. A Smooth Particle Mesh Ewald Method. J Chem Phys. 1995; 103:8577–8593.

38. Walker BJ, Krishnasastry M, Zorn L, Kasianowicz JJ, Bayley H. Functional expression of the alpha-hemolysin of Staphylococcus aureus in intact Escherichia coli and in cell lysates. J Biol Chem. 1992; 267:10902–10909. [PubMed: 1587866]

39. Tang G, et al. EMAN2: an extensible image processing suite for electron microscopy. J Struct Biol. 2007; 157:38–46. [PubMed: 16859925]

40. Maglia G, Heron AJ, Stoddart D, Japrung D, Bayley H. Analysis of single nucleic acid molecules with protein nanopores. Methods Enzymol. 2010; 475:591–623. [PubMed: 20627172]

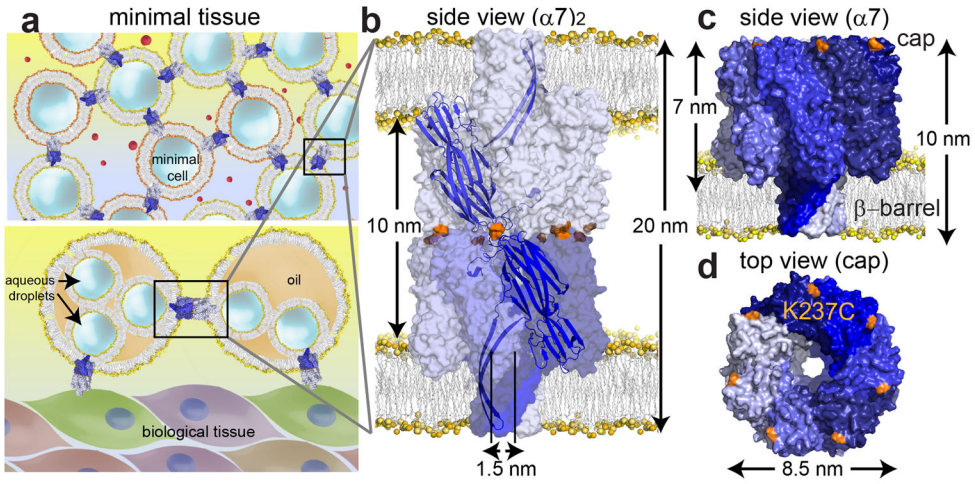

Figure 1. An engineered αHL pore dimer

(**a**) Minimal tissue models. Upper panel: minimal cells communicating through protein conduits that span both bilayers (upper panel). Lower panel: monolayer-encased droplet networks[8] interconnected and linked to biological tissues through protein conduits. (**b**) Space-filling model of the engineered pore dimer, $(\alpha 7)_2$, in which two α7 units (the normal form of the αHL pore) are linked cap-to-cap, and can span two bilayers simultaneously. (**c**) The α7 units were covalently attached through disulfide bonds between cysteine residues (orange) at position 237 in the αHL K237C mutant. The cysteine residues are located on the cap of the α7 heptamer, one on each subunit. (**d**) Top view of the cap and the location of the cysteine residue at position 237 (orange) in α7. The space filling models of α7 (PDB 7AHL) and $(\alpha 7)_2$ were created in PyMOL.

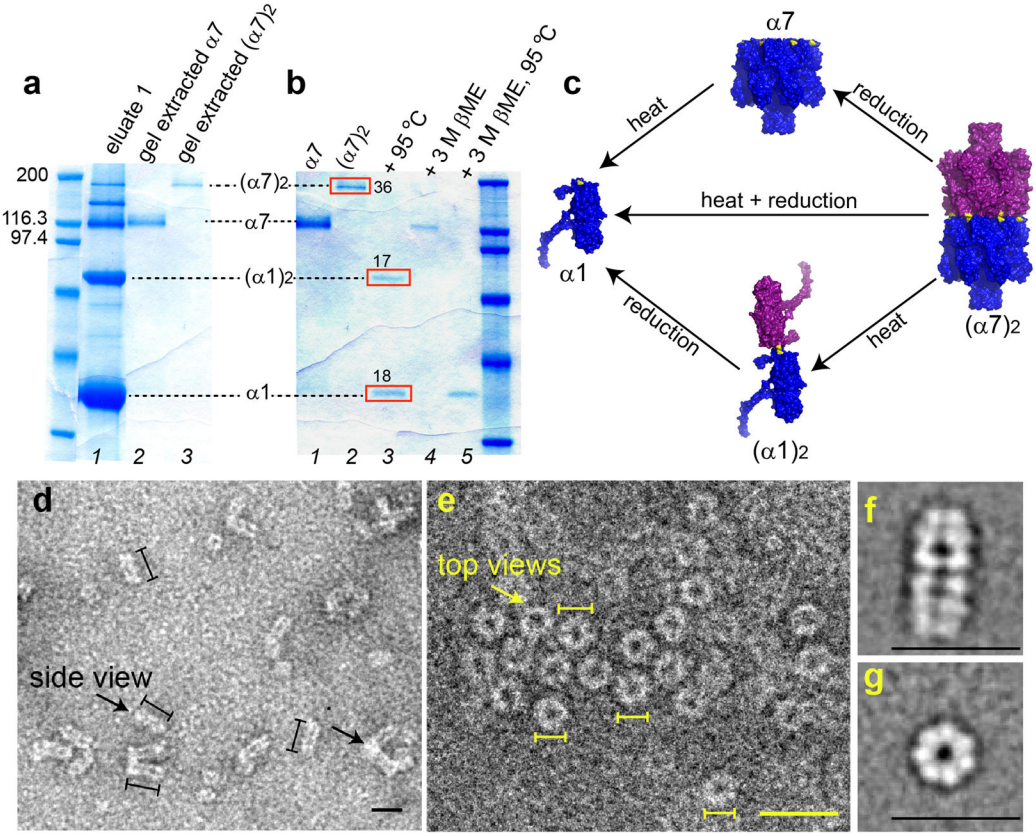

Figure 2. Expression, purification and structural characterization of $(\alpha 7)_2$

(**a**) SDS-polyacrylamide gel showing the purification of $(\alpha 7)_2$. The Ni^{2+}-NTA purified αHL mutant K237C/D8H6 contained a mixture of the monomer α1, the monomer dimer $(\alpha 1)_2$, the heptamer α7, and the heptamer dimer $(\alpha 7)_2$. α7 and $(\alpha 7)_2$ were purified (*lanes* 2 and 3) by extraction from a preparative gel (Supplementary Methods). (**b**) Heating $(\alpha 7)_2$ at 95°C for 10min yielded α1 and $(\alpha 1)_2$ (red boxes, *lane 3*) with relative band intensities of 18 and 17 absorbance units, derived from 36 absorbance units of $(\alpha 7)_2$ (red box, *lane 2*). To determine whether the $(\alpha 7)_2$ was composed of α7 units linked by disulfide bonds, a sample was treated with 3M βME for 15min at 25°C, which indeed produced α7 (*lane 4*). Upon heating at 95°C, followed by reduction with 3M βME for 15min at 25°C, $(\alpha 7)_2$ dissociated into α1 (*lane 5*). (**c**) A model for the structural composition and dissociation of $(\alpha 7)_2$ based on the electrophoresis studies. (**d**) Electron micrographs after uranyl acetate staining showing side views (*left* arrow) of $(\alpha 7)_2$ as elongated particles of length 19.6±0.2nm (mean ±s.e.m., *n*=268) and width 8.4±0.1nm (mean±s.e.m.; *n*=96), which correspond to the length (~20nm) and width (~8.5nm) of $(\alpha 7)_2$ derived from a molecular model (Fig. 1b). $(\alpha 7)_2$ particles were also observed aggregated longitudinally in clusters of three to four molecules most probably through the hydrophobic β barrel domains (*right* arrow). (**e**) Electron micrographs showing ring views of $(\alpha 7)_2$. The average diameter of the particles is 7.8±0.1nm (mean±s.e.m., *n*=131). Scale bars in **d, e**, 20nm. Lines drawn next to single particles (**d**: black; **e**: yellow) denote the boundaries used to measure lengths. (**f**) Class average of 309 single particles showing the side view. (**g**) Class average of 224 single particles showing the ring view.

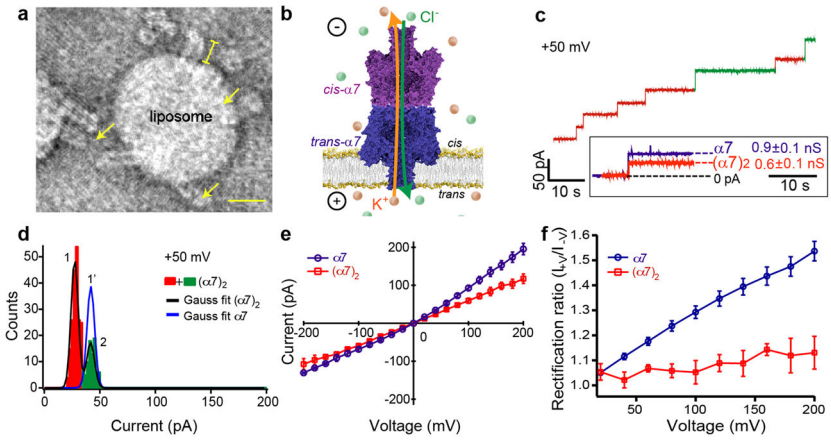

Figure 3. Electrical characteristics of $(\alpha 7)_2$

(**a**) Transmission electron microscopy (TEM) view showing $(\alpha 7)_2$ inserted into the bilayer of a liposome and seen as 17.0±0.4nm (mean±s.e.m.; *n*=131) protrusions (yellow) from the liposome surface. Scale bar, 20nm. (**b**) $(\alpha 7)_2$ was electrically characterized in planar lipid bilayers. A bilayer with an area of 1.2×10^4 to $3\times10^4 \mu m^2$ (determined by capacitance measurements) was formed on an aperture that separated two compartments, both of which contained 1M KCl, 25mM Tris.HCl, 50μM EDTA, pH8.0[40]. (**c**) A representative trace showing rapid insertion of $(\alpha 7)_2$ into a bilayer of DPhPC at +50mV. Inset shows the mean conductance (G) of the majority of the $(\alpha 7)_2$ pores (red steps) was 570±4pS (mean±s.e.m.; *n*=284, *N*=18). By comparison, α7 gave G=857±6pS (mean±s.e.m.; *n*=169, *N*=9) under the same conditions. Some $(\alpha 7)_2$ pores with unitary conductance values similar to α7 were also observed (green steps). (**d**) Histogram of the open pore currents (I_o) of $(\alpha 7)_2$ at +50mV showing the two populations (red and green). The mean I_o value of the major (red) peak was 27±4pA(mean±stdev); *n*=284, *N*=18). In comparison, the mean I_o of the minor (green) peak was 42±4pA(mean±stdev); *n*=93, *N*=18), which is similar to the mean I_o value for α7, 42±4pA (mean±stdev; *n*=169, *N*=9, blue Gaussian fit). The population of $(\alpha 7)_2$ pores with the higher mean I_o value (green) is likely to comprise “offset” structures (Supplementary Fig. S3a–c). The pores with the lower mean I_o value (red peak), 27±4pA (mean±stdev; *n*=284, *N*=18), can be assigned to structures with precisely aligned cap domains (Fig. 1b). (**e**) I–V plot for $(\alpha 7)_2$ (red) compared with that of α7 (blue) (*N*≥3). For the I–V plot of $(\alpha 7)_2$, pores with I_o values in the range of 27±4pAwere used. (**f**) Rectification ratios (I_{+V} / I_{-V}) of α7 and $(\alpha 7)_2$ were calculated as a function of applied potential.

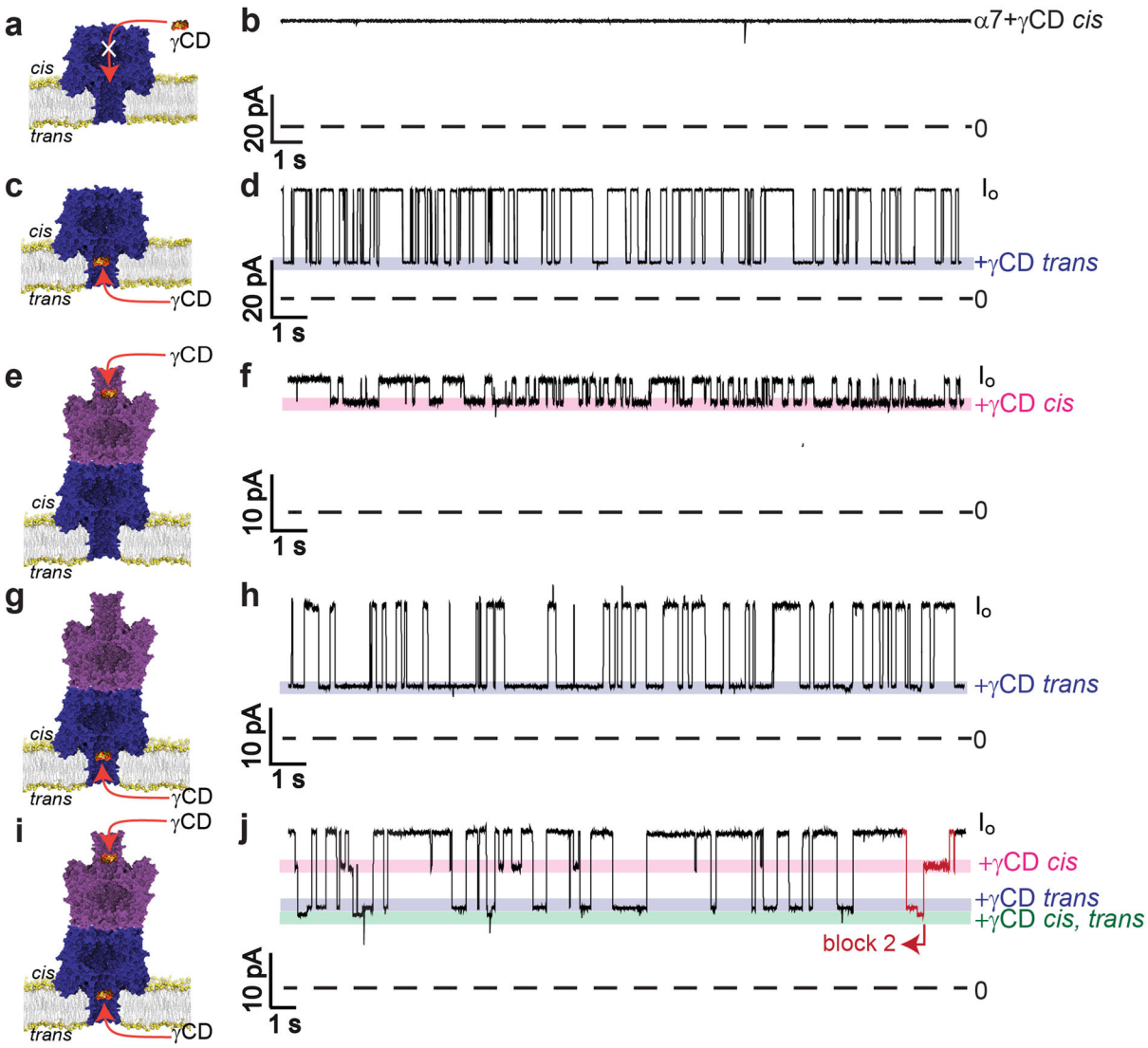

Figure 4. γ Cyclodextrin (γCD) binding to α7 and $(α7)_2$

(**a, b**) When γCD was added to the *cis* compartment, no blockades of α7 were observed. (**c**) γCD from the *trans* compartment bound within the α7 barrel and produced transient blockades. (**d**) Representative current trace showing a 66% blockade of I_o upon *trans* γCD binding to α7 at +50mV. (**e**) γCD bound to $(α7)_2$ from the *cis* compartment. (**f**) Representative current trace showing a 15% blockade of I_o upon *cis* γCD binding to $(α7)_2$ at +50mV. (**g**) γCD also bound to $(α7)_2$ from the *trans* compartment. (**h**) Representative current trace showing a 55% blockade of I_o upon *trans* γCD binding to $(α7)_2$ at +50mV. (**i, j**) 40μM γCD was added to both the *cis* and *trans* sides of $(α7)_2$ simultaneously. In this case, three blockade levels were observed, which are attributed as follows: (i) *cis* only block, 15%; (ii) *trans* only block, 55%; (iii) simultaneous *cis* and *trans* block, 61% block (n=4183, 3737 and 1121, respectively, N=6, n denotes number of individual events in N independent experiments). The simultaneous *cis* and *trans* γCD block was always preceded and followed by a *cis* only or a *trans* only block (e.g. see red part of trace: *trans* → *cis* + *trans* → *cis*). In

all traces, the blue and pink bars show the *trans* and *cis* γCD blocks, respectively. To investigate γCD binding to $(\alpha 7)_2$, only the pores with a unitary conductance of 27±4pA were used (Fig. 3d, red peak). The current traces were recorded at +50mV in 1M KCl, 25mM Tris.HCl, 50μM EDTA, pH8.0, with 80μM γCD in the *cis* and/ or *trans* compartment(s).

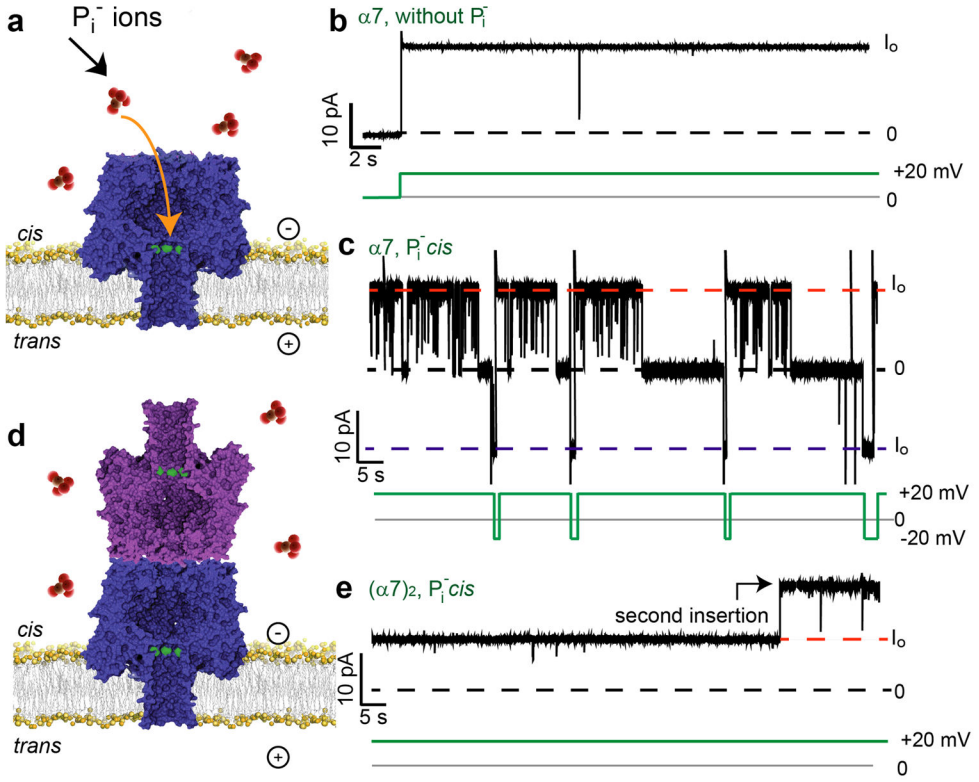

Figure 5. Phosphatebinding to M113R $(α7)_2$

(**a**) Phosphate anions (P_i, red) bind and block the heptameric pore (α7) made from M113R/K237C/D8H6 (MR) subunits from the *cis* side only. (**b**) MR α7 in the absence of P_i. (**c**) Representative current trace of a MR α7 pore with P_i in the *cis* side compartment. Transient blockades, seen as spikes, and longer blockades are observed at +20mV. The longer blockades are reversed at −20mV. (**d**) Cartoon of the cap-to-cap structure of $(α7)_2$ showing that access to the blocking site on the *trans*-α7 unit is hindered. (**e**) A representative trace of two $(α7)_2$ pores in the presence of P_i in the *cis* compartment. Neither pore bound P_i at +20mV. In **b–e**, the broken lines represent the I_o levels at +20mV (red) and − 20mV (blue), and the blocked level (black, 0pA). The green lines show the applied potential. Parts **a** and **d** are not drawn to scale. The experiments were performed in 1M KCl, 25mM Tris.HCl, 50μM EDTA, pH8.0, with 10mM sodium phosphate, pH8.0 as noted.

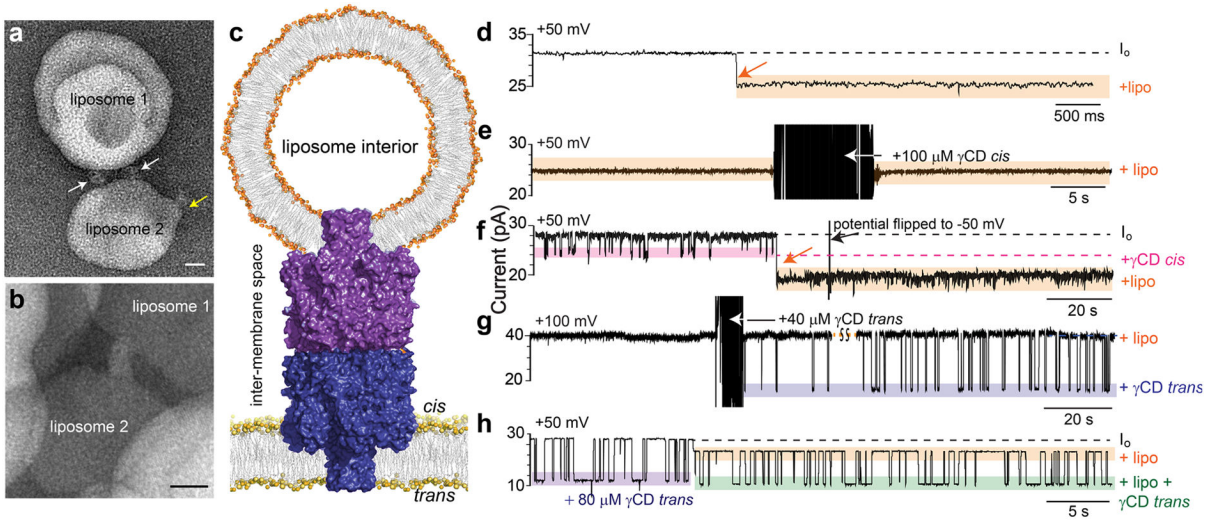

Figure 6. Simultaneous insertion of $(\alpha 7)_2$ into two adjacent lipid bilayers

(a, b) TEM images of $(\alpha 7)_2$ inserted into two liposomes simultaneously. $(\alpha 7)_2$ was mixed with (**a**) 10 mol% POPG: POPC liposomes or (**b**) egg-PC liposomes in lipid to protein ratios of 20:1 (w/w) and 100:1 (w/w), respectively. (**c**) Insertion into two bilayers was observed in single-channel electrical recordings. Cartoon (not to scale) showing $(\alpha 7)_2$ with its *cis*-α7 barrel inserted into a unilamellar liposome and the *trans*-α7 barrel inserted into a planar lipid bilayer. (**d–h**) Representative electrical traces of liposome insertion or liposome-inserted $(\alpha 7)_2$ pores. (**d**) Insertion of the *cis*-α7 barrel of $(\alpha 7)_2$ into a unilamellar liposome is observed as an irreversible block of I_o of 23±1% (percentage block of I_o±s.e.m.; N=12) at +50mV. (**e**) An $(\alpha 7)_2$ pore that had inserted into a liposome did not display any *cis* γCD (100 μM) binding events at +50mV. (**f**) C*is* γCD blockades cease after insertion into a liposome at +50mV. The liposome block could not be reversed by flipping the potential to −50mV. (**g**) Upon the addition of γCD (40 μM) to the *trans* side of an $(\alpha 7)_2$ pore that had inserted into a liposome, transient binding events (purple box) were detected (+100mV). (**h**) If γCD was present on the *trans* side of $(\alpha 7)_2$ before liposome insertion, *trans* γCD binding events (purple box) continued (green box) after liposome insertion at +50mV. The experiments were performed in 1M KCl, 25mM Tris.HCl, 50μM EDTA, pH8.0, withγCD (*cis* or *trans*; concentration as noted) and/ or liposomes (2.5mg mL^{-1}, *cis*), as noted.

Table 1

Kinetic and equilibrium dissociation constants for the interaction of γCD with $(\alpha 7)_2$ and α7

The rate constants values were obtained from at least three different experiments, in each of which at least three γCD concentrations were used in 1M KCl, 25mM Tris.HCl, 50μM EDTA, pH8.0 at 25°C. At each voltage, the dissociation rate constants, k_{off}, were derived at each γCD concentration as the inverse of the mean residence time (τ_{off}) of γCD within the pore. The mean value over all concentrations is given in the Table. The association rate constants, k_{on}, were obtained for each experiment from the slope of a plot of the inverse of the mean inter-event interval (τ_{on}) versus γCD concentration. The dissociation constants (K_d) were calculated separately for each experiment from $K_d = k_{off} / k_{on}$. The mean values of K_d for three or more experiments are reported in the Table.

Voltage (mV)	**$k_{on} \times 10^4$ (M^{-1} s^{-1})**	**k_{off} (s^{-1})**	**K_d (μM)**	**blockade of I_o**
$(\alpha 7)_2$*trans*	(mean±s.e.m)	(mean±s.e.m)	(mean±s.e.m)	(mean±s.e.m)
+40	7.1±0.7	3.7±0.4	49±3	55±2
−40	8.2±1.1	3.2±0.2	36±2	51±2
+50	9.0±1.1	3.4±0.4	42±3	55±2
−50	6.1±0.6	3.3±0.3	54±8	48±3
+100	8.9±1.0	4.2±0.8	46±7	54±5
−100	4.5±0.3	2.9±0.5	64±11	45±6
$(\alpha 7)_2$*cis*				
+40	5.8±0.8	6.0±0.4	85±12	16±2
−40	5.6±0.5	7.2±1.1	110±18	17±1
+50	6.0±0.5	6.9±0.7	110±12	15±1
−50	6.1±1.0	6.2±1.0	96±9	19±1
+100	6.3±1.2	6.4±2.0	110±27	13±0.3
−100	6.4±1.3	10±1.6	130±24	21±2
α7 *trans*				
+40	9.5±1.2	6.1±0.7	76±12	65±1
−40	5.0±0.1	3.1±0.4	61±6	58±1
+50	7.8±0.9	6.9±0.9	110±37	66±1
−50	7.2±2.3	3.0±0.3	47±9	58±0.4
+100	4.3±1.2	12.3±2.0	342±63	68±0.3
−100	6.9±2.8	1.7±0.2	37±10	52±0.1